IN THIS ISSUE

Barcoded FACS samples

Flow cytometry is a dream come true for anybody interested in rapidly measuring multiple parameters on every single cell in a large cohort. Advances in the development of antibodies against cell-surface proteins and intracellular signaling molecules, and sophisticated cytometers with multiple lasers have increased the number of markers one can measure for each cell. Nolan and colleagues now take the information to be gleaned in one cytometry run a step further. By barcoding differently treated samples with dilutions of fluorescent dyes, they create a unique signature for every treatment, then combine all samples and analyze them in a single tube. To interpret the data they deconvolute the results and obtain measurements for each marker in each distinct population. The practical fallout of the barcoding technique is a considerable savings in time and reagent cost, which can then be translated into the screening of large libraries of compounds for their effect on cellular behavior.
Article p361, News and Views p343

Finding patterns in rapid neuronal firing

Sensory stimuli trigger complex patterns of neuronal action potentials in the brain. Measurement of these patterns is important for understanding the way the brain processes information. There are currently no efficient techniques to visualize patterns of high-frequency action potentials. Because individual action potentials result in transient increases in intracellular Ca^{2+}, fluorescent calcium sensors are often used as an indirect readout of these spikes. Because of the slow decay of Ca^{2+} signals, however, Ca^{2+} remains elevated during high-frequency firing, making it difficult to determine the underlying changes in firing rate. Yaksi and Friedrich now report a signal-processing method that uses deconvolution to accurately determine changes in action potential firing rate that underlie Ca^{2+} signals visualized by two-photon microscopy in whole brain.
Article p377, News and Views p344

Programmed nonnatural peptide synthesis

Methods to reprogram the genetic code to incorporate non-natural amino acids are powerful tools for constructing polypeptides with unique labels or structural properties. The Suga laboratory has pioneered the application of a *de novo* ribozyme-like molecule, Flexizyme, to facilitate the coupling of acyltRNAs with non-natural amino acids. Now Suga and colleagues have developed two new Flexizymes, dinitro-Flexizyme and enhanced Flexizyme, which together provide nearly unlimited recognition and incorporation of amino or hydroxy acids. When the Flexizymes are used in a cell-free translation system, peptides integrating multiple non-natural amino acids can be synthesized.
Brief Communication p357

RNAi screening goes live

RNA interference (RNAi) is a powerful method to determine the function of specific genes and proteins by triggering degradation of target mRNAs. But the methods of measuring the effect of gene knockdown by RNAi now rely on end-point assays. Therefore, these assays may miss important or complex transient phenotypes. Ellenberg and colleagues describe a combination of on-chip short interfering RNA transfection and live-cell fluorescent imaging for high-throughput screening of large numbers of gene knockdown phenotypes. Visualizing the effect of RNAi in real-time using live cells offers a valuable addition to what is currently achievable with end-point assays.
Article p385

Designing multicellular networks in 3D

The natural environment of cells *in vivo* is a three-dimensional (3D) network in which cellular responses are determined by influences from surrounding cells on all sides—a complex system that cannot be recapitulated in a traditional, two-dimensional Petri dish. Bhatia and colleagues took on the challenge of constructing a precisely defined 3D cellular network, developing a new cell patterning technique that formed cell clusters of specified size and shape and immediately embedded them in an organic hydrogel. Using this method, they studied the effect of cell cluster size on the regulation of chondrocyte biosynthesis over the course of several weeks—and showed for the first time that cell proximity alone may have biological consequences. The ability to design 3D cell architecture represents progress toward more biomimetic cell culture and will aid in the deciphering of cellular communication that takes place in three dimensions.
Article p369

Probing the role of multicellular organization in three-dimensional microenvironments

Dirk R Albrecht[1,2], Gregory H Underhill[1,2], Travis B Wassermann[1], Robert L Sah[1] & Sangeeta N Bhatia[1–3]

Successful application of living cells in regenerative medicine requires an understanding of how tissue structure relates to organ function. There is growing evidence that presentation of extracellular cues in a three-dimensional (3D) context can fundamentally alter cellular responses. Thus, microenvironment studies that previously were limited to adherent two-dimensional (2D) cultures may not be appropriate for many cell types. Here we present a method for the rapid formation of reproducible, high-resolution 3D cellular structures within a photopolymerizable hydrogel using dielectrophoretic forces. We demonstrate the parallel formation of >20,000 cell clusters of precise size and shape within a thin 2-cm^2 hydrogel and the maintenance of high cell viability and differentiated cell markers over 2 weeks. By modulating cell-cell interactions in 3D clusters, we present the first evidence that microscale tissue organization regulates bovine articular chondrocyte biosynthesis. This platform permits investigation of tissue architecture in other multicellular processes, from embryogenesis to regeneration to tumorigenesis.

Mammalian cells integrate and respond to cues in the microscale environment, such as cell shape and organization, contacts with neighboring cells as well as chemistry and mechanics of the surrounding fluid and extracellular matrix. Hence, cellular signaling is often altered in tumor cells[1,2], stem cells[3] and differentiated cells[4] when cultured on flat, adherent substrates that lack structural cues. Although microfabrication tools have been developed to uncouple some of these regulatory signals in adherent cultures[5,6], similar methods in more physiological 3D systems have not yet been available. To date, *in vitro* 3D model systems typically embed cells or cell spheroids within tissue-like hydrogels[2,4,7,8], but are limited by slow spontaneous aggregation of spheroids with poorly controlled size and shape[3,9].

Our goal was to precisely organize cells using external physical forces (for example, optical, electromagnetic, fluidic forces) rather than spontaneous aggregation, and then to rapidly 'trap' newly formed 3D structures in a biocompatible, stimuli-sensitive (for example, pH, temperature, light) hydrogel. We chose dielectrophoretic (DEP) forces for cell manipulation and a photopolymerizable polyethylene glycol (PEG) hydrogel for tissue formation. DEP forces arise when polarizable particles are subjected to a nonuniform electric field and have been widely used for dynamic manipulation of biological objects[10–12] (for example, cell separation) and more recently for stable trapping[13]. Synthetic hydrogels such as PEG offer the ability to tune bioactivity, porosity, degradation and gelation trigger[14], and photopolymerizable hydrogels have been conveniently used as inert biomaterials or to entrap randomly dispersed cells as tissue constructs[7,8,15]. By adapting and combining these techniques, we report the ability to fabricate and study tissues with varying microstructure (that is, cluster size, shape and spacing). Furthermore, we demonstrated that cell microorganization has biological consequences independent of culture geometry, chemistry or volumetric cell density. In particular, we investigated the role of 3D microorganization in bovine articular chondrocytes, one of many cell types with altered behavior in adherent culture[4] that would not be amenable to previous micropatterning methods.

RESULTS

Formation of hydrogels containing 3D-microorganized cells

The DEP cell patterning (DCP) chamber used in our experiments (**Fig. 1a**) sandwiched a suspension of cells in un-cross-linked prepolymer solution between two conductive indium tin oxide (ITO)-coated glass slides. On the bottom 'electrode array' slide, a thin micropatterned layer of insulating photoepoxy (SU-8) masked most of the conductive surface to form 'electrodes' in all remaining uninsulated areas. An alternating current (a.c.) bias applied across the top and bottom surfaces produced a spatially nonuniform electric field that was strongest near the gaps in the dielectric layer (**Fig. 1b**). Dielectrophoretic forces propelled cells toward locations of high electric field strength, and cell motion was complete within 1–3 min (**Supplementary Fig. 1** online and **Supplementary Videos 1** and **2** online). After cell localization, ultraviolet (UV) light exposure through the transparent chamber covalently crosslinked the hydrogel, thereby entrapping newly formed multicellular structures. We then transferred the 'DCP hydrogel' containing an embedded micropattern of living cells from the chamber to standard culture plates and medium. The complete process required only ~20 min.

[1]Department of Bioengineering, University of California–San Diego, La Jolla, California 92037, USA. [2]Harvard–Massachusetts Institute of Technology Division of Health Sciences and Technology & Electrical Engineering and Computer Science, Massachusetts Institute of Technology, Cambridge, Massachusetts 02139, USA. [3]Brigham and Women's Hospital, Boston, Massachusetts 02115, USA. Correspondence should be addressed to S.N.B. (sbhatia@mit.edu).

RECEIVED 6 DECEMBER 2005; ACCEPTED 17 MARCH 2006; PUBLISHED ONLINE 20 APRIL 2006; DOI:10.1038/NMETH873

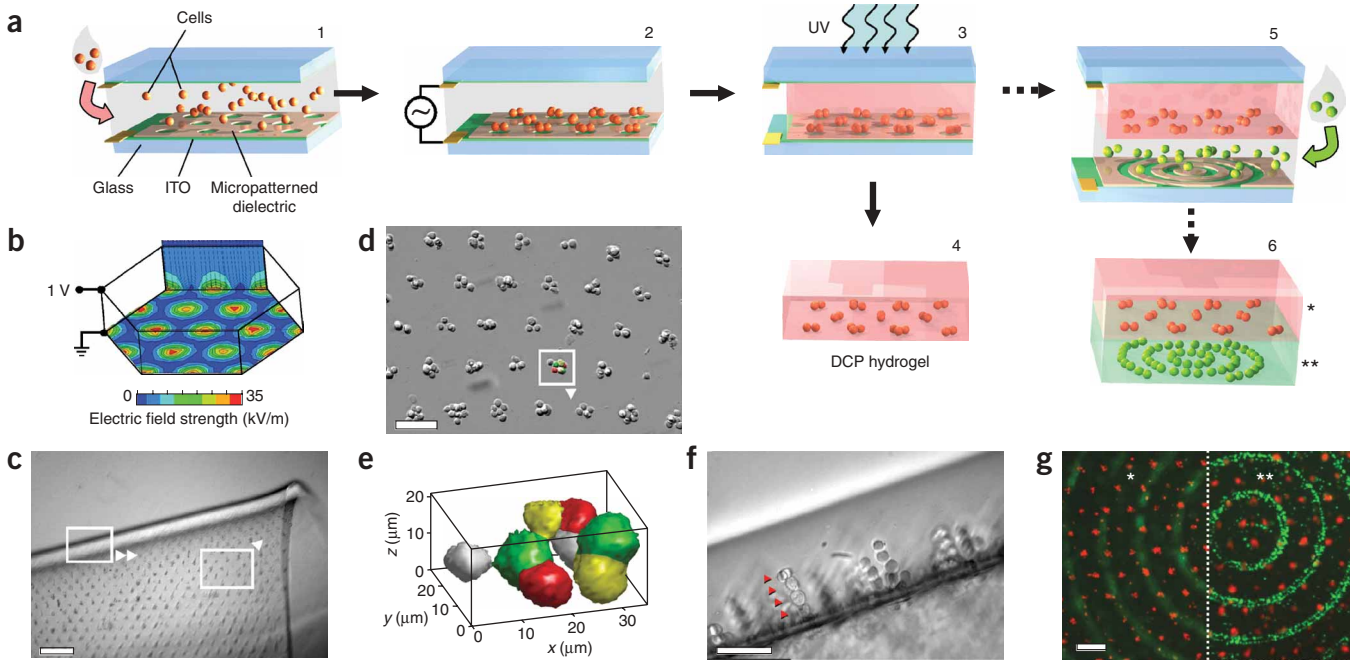

Figure 1 | Fabrication method and examples of DCP hydrogels. (**a**) Cells in prepolymer solution are introduced into the transparent chamber (1) and localize via dielectrophoretic forces to micropatterned gaps in the 1.8-μm-thick dielectric layer upon application of the a.c. chamber bias (2). Next UV light exposure polymerizes the hydrogel (3), embedding cells in a stable microorganization. The 'DCP hydrogel' can then be removed and cultured (4) or incorporated into multilayer constructs by expanding the chamber height and repeating steps 1–3; each layer may contain distinct cell organization, cell type and hydrogel formulation (5, 6). (**b**) Electric field strength is high above circular gaps in the dielectric layer arranged in a hexagonal array (100-μm spacing), as shown by finite element modeling (CFD Research Corp.). (**c**–**f**) The 100-μm-thick DCP hydrogels contain a microarray of embedded fibroblast clusters. In **c**, the free-floating hydrogel is shown folded; boxes indicate orientation of panels **d** and **f**. In **e**, the 3D shape of an 8-cell cluster from **d** is rendered from confocal data (MATLAB; pseudocolored to depict individual cells). Cross-sectional view of linear columns 4–5 cells long (arrowheads) demonstrates cluster shape versatility (**f**). (**g**) A bilayered hydrogel (200 μm total thickness) contains distinct fluorescently labeled fibroblasts in a cluster array above (*) and in concentric rings below (**), as depicted in **a** (step 6). The same microscope field is shown focused on the upper or lower cell pattern, as delineated by the dotted line. Scale bars: **c**, 250 μm; **d**,**g**, 100 μm; **f**, 50 μm.

To illustrate the capabilities of this method, we organized mouse fibroblasts into a hexagonal array of cell clusters, 100 μm apart, within a thin hydrogel (**Fig. 1**, **Supplementary Fig. 1** and **Supplementary Video 1**). The hydrogel thickness, precisely defined by the silicone gasket, minimized mass transport barriers that can occur in 3D hydrogel models and allowed compatibility with high-resolution inverted microscopy. A typical 10 × 20 × 0.1 mm DCP hydrogel contained >20,000 repeated cluster units at an area density of 115 clusters/mm^2. Cellular microstructures remained stable within the thin hydrogel, even upon large deformations (**Fig. 1c**). Encapsulated cells within clusters were rounded and positioned in close proximity to neighboring cells (**Fig. 1d**,**e**). Notably, we were able to manipulate cluster shape in three dimensions from spheroids penetrating ~20 μm into the hydrogel (**Fig. 1d**,**e**), to linear cell columns over 50 μm tall (**Fig. 1f**). This organizational diversity is due to the influence of field-induced cell-cell attraction (known as "pearl chaining"[10]), and flatter clusters reproducibly occurred when cells settled before we energized the chamber (**Supplementary Fig. 2** online).

The ability of photolithography to pattern arbitrary shapes in the insulating layer on the 'electrode array' affords considerable versatility in specifying cellular microstructures. For example, we organized cells in concentric circles (**Fig. 1g**), parallel lines, branching networks and radial chords (**Fig. 2**). We found excellent correspondence between the designed photomask geometry (used to fabricate the electrode array) and the entrapped cellular patterns (**Fig. 2**). One can engineer further organizational complexity with distinct cell types and/or hydrogel formulations in each layer of multilayer constructs[16], as demonstrated here with a bilayered DCP hydrogel (**Fig. 1g**). Other applications of the layer-by-layer process include additive fabrication of complex tissues and investigation of the interplay between different encapsulated cell types.

To demonstrate biological versatility of the DCP method, we patterned a variety of mammalian cell types, including differentiated primary cells (rat hepatocytes, bovine chondrocytes) and cell lines (3T3 fibroblasts, human HepG2, HeLa), and uncommitted progenitors (bipotential mouse embryonic liver (BMEL) cells; **Fig. 2**). The method is also compatible with any encapsulating biomaterial that meets the criteria for rapid dielectrophoretic patterning[17], in particular, low prepolymer viscosity, a controllable gelation trigger, and sufficient hydrogel strength and stability to retain cell patterns for the experiment duration. We demonstrated the patterning method in agarose (**Fig. 2h**,**i**), a biomaterial commonly used for cell encapsulation with very distinct properties from the PEG hydrogel. In contrast to the synthetic, photosensitive, covalently crosslinked and nondegradable PEG hydrogel, agarose is naturally derived, forms a noncovalent large-pore macroreticular network via thermoreversible gelation and is enzymatically degradable.

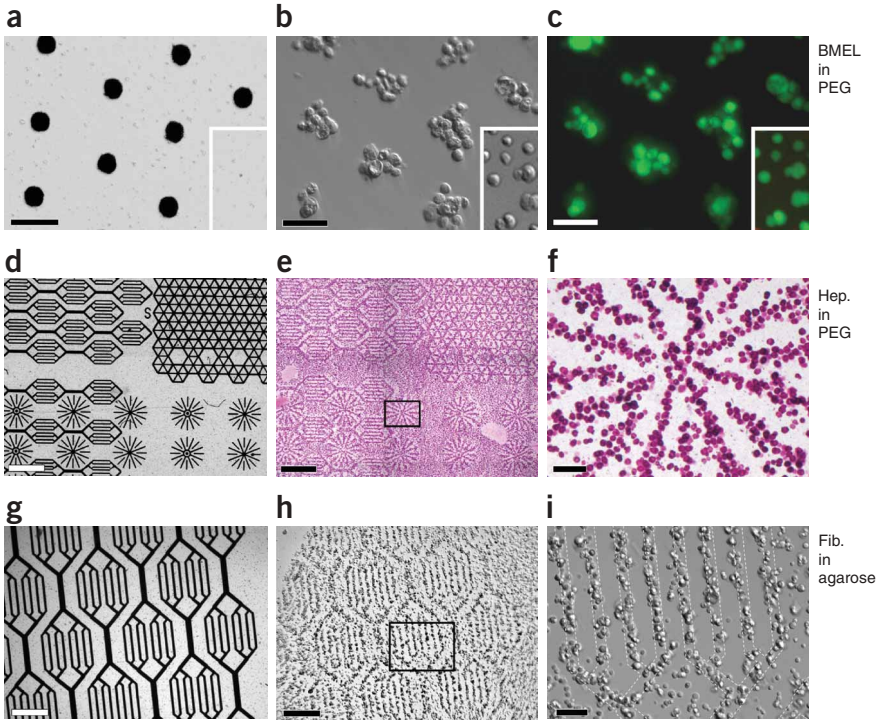

Figure 2 | DCP versatility in cell type, micropattern and hydrogel chemistry. (**a**–**c**) BMEL cells, which remain undifferentiated in adherent monolayer culture but upregulate liver-specific functions in spheroid culture[30], were patterned in clusters within a PEG hydrogel and stained with a vital dye (**c**). Unpatterned cells within the same hydrogel showed identical viability (insets). (**d**–**f**) Primary rat hepatocytes patterned in various biomimetic microstructures within a PEG hydrogel stain specifically for intracellular glycogen via the periodic acid–Schiff stain (**e**,**f**). (**g**–**i**) DCP hydrogels were also formed via thermal gelation of 1% (wt/vol) agarose. After cell patterning at 25–37 °C, the chamber was cooled in ice water to form a stable, 200-μm-thick agarose hydrogel containing encapsulated fibroblasts. Boxed regions (**e**,**h**) are magnified in panels **f** and **i**. Photomask patterns (**a**,**d**,**g**) used to fabricate the electrode arrays closely matched the resulting cell patterns (**b**,**e**,**h**). Scale bars: **a**–**c**, 50 μm; **d** and **e**, 1 mm; **g** and **h**, 500 μm; **f** and **i**, 100 μm.

Characterization of cell microorganization

To study the global impact of microscale tissue organization, it is imperative that the technique reproducibly and efficiently forms microstructures of predictable size and shape. Our strategy was to use a closed chamber without fluid flow to collect all cells within a defined volume as a cluster above each electrode. As expected, the distribution of cluster size matched a Poisson distribution (**Fig. 3**), reflecting cell localization from random initial positions to regularly spaced electrodes. The theoretical mean cluster size and standard deviation,

$$\bar{N}_{cl} = \rho h/\Delta = \rho\frac{\sqrt{3}}{2}s^2 h, \sigma_{cl} = (\bar{N}_{cl})^{1/2} \quad (1)$$

closely predicted measured values (coefficient of variation (c.v.) = 3.8%) from volumetric cell suspension density (ρ), chamber height (h), and area electrode density (Δ) or spacing between hexagonally packed electrodes (s). Simple variation of cell seeding density produced repeatable distributions of cluster size, from single cells to >30 cells, using an array of fixed electrode spacing (**Fig. 3**). Notably, equation (1) also predicts that cluster size is influenced by the square of electrode spacing, a highly tunable parameter. We confirmed this experimentally in a single electrode array with domains of distinct electrode spacing, forming three cluster sizes ranging from 3.7 to 17.0 cells (**Fig. 4**). Cells within a fourth quadrant, which did not contain gaps in the dielectric layer, experienced a weak uniform electric field and cell-cell repulsive force that dispersed them into an 'unclustered' organization (**Fig. 4** and **Supplementary Fig. 2**). Analysis of multiple microorganizations within a single DCP hydrogel is advantageous, ensuring identical cell source and treatment as well as hydrogel chemistry.

Characterization of cell viability

Both dielectrophoresis and hydrogel polymerization have the potential to damage living cells. In our system, the high a.c. bias frequency minimized transmembrane potentials induced by the electric field (**Supplementary Fig. 3** online) and the low-conductivity buffer eliminated Joule heating. For photopolymerization experiments, we and others have reported a cell-type dependent sensitivity to light exposure, photoinitiator type and concentration, medium formulation, and hydrogel chemistry[7,16,18]. By optimizing each parameter for these studies, DCP hydrogels containing bovine chondrocytes demonstrated high viability at day 1 (94 ± 3%) and day 14 (80 ± 7%) relative to the initial suspension (97 ± 2%; **Fig. 4c**). Viability was constant across cluster sizes (c.v. ≤ 1.3% through day 14), further suggesting minimal cytotoxic

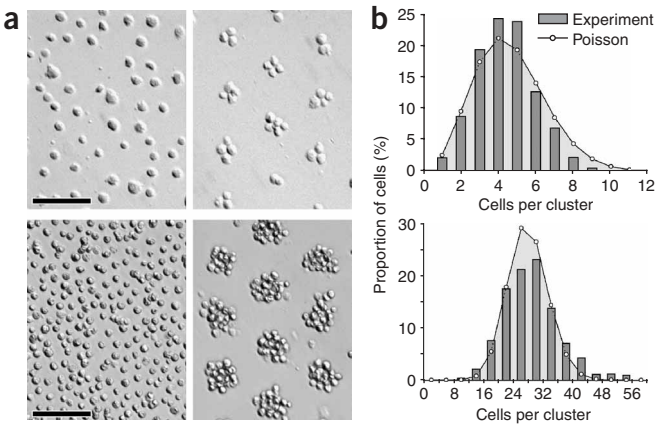

Figure 3 | Quantitative control of cell microorganization within DCP hydrogels. (**a**) Mean cell cluster size is predictable and proportional to seeding density (4 million/ml, above; 30 million/ml, below). Phase micrographs depict cell organization before (left) and after patterning into clusters (right) using an identical chamber for both cell densities. Using electrodes with subcellular dimensions, single cells can also be precisely patterned[13]. Scale bars, 100 μm. (**b**) Histograms of cluster size, quantified from the same hydrogels shown in **a**, consistently followed a Poisson distribution.

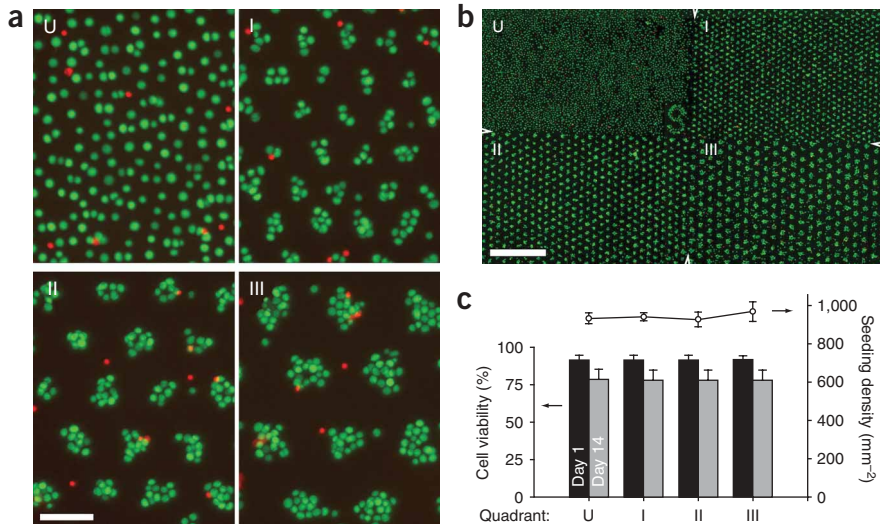

Figure 4 | Multiorganization DCP hydrogels containing viable cells. (**a**,**b**) Mean cell cluster size increases by the square of cluster spacing. A single DCP hydrogel with uniform cell density (**b**) is shown containing four quadrants of distinct cluster size (magnified in **a**). Quadrants I–III have 3.7, 8.7, and 17.0 mean cells per cluster at 65, 100 and 140 μm spacing, respectively. Quadrant U contains individual 'unclustered' cells. Thus, various cell microorganizations can be studied simultaneously, ensuring identical hydrogel chemistry and cell source. Fluorescent staining distinguishes viable (green) from nonviable (red) cells. Scale bars: **a**, 100 μm; **b**, 1 mm. (**c**) Area cell density and high chondrocyte viability were uniform across all organizations at both day 1 (black bars) and day 14 (gray bars). Data are mean ± s.d., $n = 12–14$.

effects of the DCP protocol. Notably, nonviable cells did not participate in microstructures of interest (**Fig. 4**), owing to reduced dielectrophoretic forces as electrical properties equalized across the damaged cell membranes.

Cell microorganization regulates chondrocyte biosynthesis

To demonstrate the biological potential of the DCP tool, we investigated the role of microscale organization in a model of articular cartilage. Chondrocytes produce matrix molecules, primarily proteoglycans and type II collagen, which are largely responsible for the mechanical properties of cartilage. Cartilage tissue contains well-defined multicellular structures that vary *in vivo* with developmental stage, anatomic zone (for example, superficial clusters near articulating surfaces and columns in deeper zones), and disease (for example, large clonal clusters in osteoarthritic and repair tissues)[19,20]. Although soluble, insoluble and mechanical factors are known to regulate chondrocyte biosynthesis and cell fate[21,22], the causative influence of cell microorganization on chondrocyte behavior has not been established. Thus, our first biological demonstration of DCP tested the hypothesis that 3D chondrocyte microorganization (a previously inaccessible independent variable) would alter subsequent matrix biosynthesis. Two further motivations for this study design were: (i) the unique capability of DCP to investigate microscale 3D organization in cartilage because of the phenotypic instability of chondrocytes in flat '2D' culture[4], and (ii) the well-characterized function of chondrocytes in unpatterned, photopolymerized hydrogels[7,8].

We isolated articular chondrocytes from immature bovine femoral condyles and incorporated them into DCP hydrogels containing four quadrants of distinct cell organization: as individual cells or in clusters of 3 to 18 cells each (**Fig. 5**). Hydrogels contained a single patterning layer to permit microscopic evaluation of cell viability and biosynthetic function. Patterned cells experienced the electric field for 6.5 ± 0.3 min and UV light exposure (1.95 mW/cm^2) for 3.5 min. We estimate that field-induced transmembrane potentials did not exceed

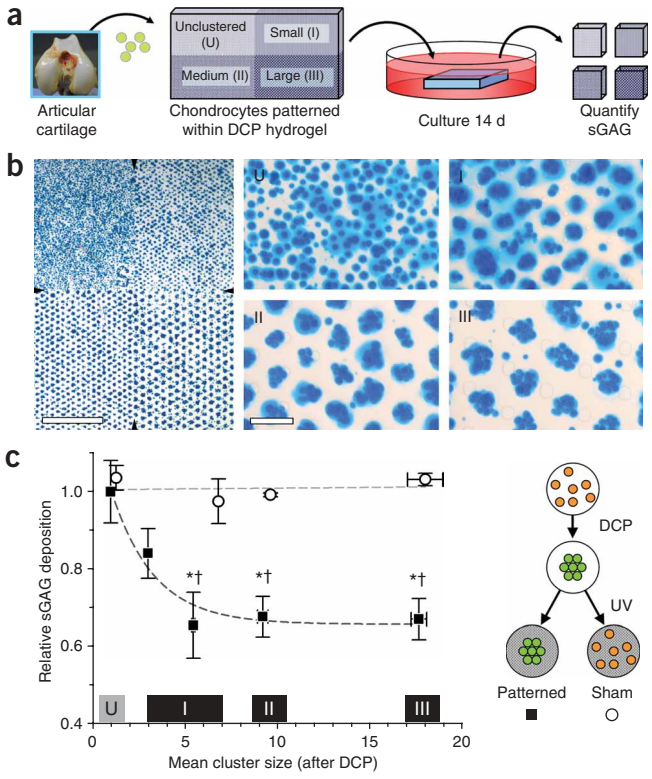

Figure 5 | Regulation of matrix biosynthesis by chondrocyte cluster size. (**a**) Articular chondrocytes incorporated into 10 × 20 × 0.1 mm DCP hydrogels were assayed for cumulative 14-d deposition of a model biosynthetic product, sGAG. (**b**) Each hydrogel contained four cell microorganizations with variable chondrocyte cluster size (1–18 cells) but constant volumetric cell density (10 million cells/ml). Blue staining indicates local sGAG deposition in whole-mount brightfield micrographs. High-magnification panels (right) show matrix deposition for each cell organization of a single typical hydrogel (left). Scale bars, 1 mm (left); 100 μm (right). (**c**) Chondrocytes patterned in clusters (I–III) deposited less sGAG per cell than matched unclustered controls (U) in a dose-dependent manner that reached a plateau for clusters >5 cells (filled squares). 'Sham'-patterned hydrogels, that is, exposed to the electric field but dispersed to a random organization before cross-linking, were indistinguishable from unclustered controls regardless of initial cluster size, indicating minimal effects of the DCP process (open circles). *, $P < 0.001$ versus control (U); †, $P < 0.001$ versus 'sham' for each organization group. Data are mean ± s.e.m., $n = 5–6$ (patterned); $n = 2–4$ (sham).

2.2 mV_{rms} (for individual cells) or 13.3 mV_{rms} (in quadrant II), far below typical cell resting potential (**Supplementary Fig. 3**). Cell viability and volumetric seeding density were constant across all cluster sizes during the 14-d experiment (**Fig. 4c**), and proliferation in the nondegradable hydrogel was minimal (5 ± 1%; **Supplementary Fig. 4** online).

Matrix molecules secreted by embedded chondrocytes become trapped in the PEG hydrogel[8] (**Fig. 5b**). Therefore, we separated each DCP hydrogel quadrant into fragments after 14 d for analysis of sulfated glycosaminoglycan (sGAG), a model biosynthetic product of differentiated chondrocytes. Cumulative sGAG deposited per cell decreased in a dose-dependent manner with increasing cluster size, reaching a plateau of 67 ± 5% (s.e.m.) at >5 cells relative to unclustered cells ($P < 0.001$), with half of the effect occurring at approximately 3 cells per cluster (**Fig. 5c**). As a control, we formed 'sham' DCP hydrogels by organizing cells under an applied electric field as above (2.26 ± 0.07 Vrms, 5 MHz for 6.1 ± 0.7 min), but then removing the field for ~30 s to rerandomize cells before photoentrapment. These unclustered but electric field-exposed control cells showed no difference in sGAG deposition for any initial cluster size, reflecting that chondrocyte biosynthesis (not subtle electric field effects) specifically modulated microscale organization. These results are consistent with our viability data (**Fig. 4**) and with previous reports describing the minimal effects of short-duration, high-frequency electric fields on cell viability, cell cycle parameters and gene expression[13,23,24].

DISCUSSION

Collectively, these data represent the first effort to control 3D microscale organization of chondrocytes as an independent variable. Prior comparisons of chondrocytes in various organizations were coupled to different chemical and mechanical environments, such as histological examination of cartilage explants and micromass culture of chondrocytes with or without pericellular matrix[25]. Chondrocytes embedded randomly within various defined hydrogels favored proliferation at lower seeding density and matrix biosynthesis at higher cell density[26,27]. If one likens our large cell clusters to hydrogels of high volumetric cell density, one would expect the opposite trends from those reported here (that is, increased rather than decreased biosynthesis in larger cell clusters). By uncoupling volumetric cell density (and attendant covariables such as nutrient transport and paracrine signaling) from local cell organization, we could attribute changes in sGAG deposition to differences in cellular organization rather than indirect correlations with cell source, viability or fate. Moreover, the biosynthetic effect was sensitive to very small changes in cell spacing (<10 μm); for example, clustered cells were mostly in contact with neighboring cells, whereas unclustered cells had a membrane separation of 9 ± 5 μm (quadrant II versus U in **Fig. 5b,** and **Supplementary Fig. 5** online).

Establishing the influence of microscale organization on cell fate has practical as well as scientific implications. For tissue engineering applications, one might expect more rapid matrix synthesis by chondrocytes in high density, randomly seeded hydrogel scaffolds than in micromass pellets. These results also support a possible role of chondrocyte microorganization in osteoarthritic cartilage or repair tissue after injury[28], characterized by abnormal clonal clusters and low proteoglycan content that contributes to poor mechanical tissue properties[20].

To explore the mechanism by which cell clustering in 3D downregulates matrix biosynthesis, we performed parallel DCP experiments using chondrocytes surrounded by a ~3 μm layer of pericellular matrix formed during 2 weeks of alginate culture (**Supplementary Methods** online). In these cells, which were incapable of forming direct cell membrane contacts, the inhibitory effect of cell clustering on sGAG deposition diminished fourfold over identical cells in which we had enzymatically removed the matrix layer. This result is consistent with either direct cell-cell contact or indirect signaling via secreted pericellular matrix molecules, as soluble proteoglycan (including sGAG) has been reported to downregulate sGAG biosynthesis[29]. We hypothesize that microscale organization may have a multifactorial role in chondrocyte behavior, analogous to 2D model systems of hepatic tissue microorganization in which soluble factors, cell-matrix interaction and direct cell contact together determine emergent tissue properties[5]. Notably, the DCP method provides a comprehensive framework for further investigation and decoupling of these microenvironment variables, by controlling 3D cell organization and contact independent of insoluble factors and physical forces (the hydrogel) and soluble signals (the culture medium).

This study provides the essential first steps in exploring the role of microscale organization of tissues in three dimensions. The DCP hydrogel system is versatile, rapidly yielding reproducible clusters of prescribed shape, size and distribution. The thin hydrogel geometry facilitates nutrient transport, is amenable to scale-up, and is compatible with *in situ* assays via standard and confocal microscopy (for example, with nondestructive reporters and fluorescent probes, histological stains, immunolabels) as well as bulk assays of cell function and gene expression (for example, colorimetric or radiolabel assays, RNA extraction and reverse transcriptase–PCR, protein extraction and enzyme-linked immunosorbent assay; ELISA). DCP hydrogels retain the chemical and mechanical tunability of the encapsulating biomaterial, and are readily implantable for *in vivo* experimentation. The DCP method effectively patterns any cell type, including specialized cells in which 3D culture microorganization or cell-cell interaction has been implicated in cell behavior, such as stabilization of primary hepatocytes[5] and differentiation of embryonic liver progenitors[30] (**Fig. 2**). The selection of appropriate patterning conditions (**Supplementary Fig. 3** and ref. 17) resulted in long-term viability and differentiated cell function. This study focused on large-scale arrays of varying 3D cluster size, a useful pattern for modulating cell-cell interaction. We further demonstrated the ability to produce arbitrary hydrogel-encapsulated cell patterns for other experimental designs and multilayer hydrogels for co-culture or tissue engineering applications. In our view, new model systems such as this one are necessary to define the structure-function relationships of multicellular systems to realize the full potential of living cells, including stem cells, as therapeutic entities.

METHODS

Device fabrication and operation. The DCP chamber comprised two indium tin oxide (ITO)-coated conductive glass slides (Delta Technologies) separated by a thin silicone gasket (XP-476; Silicones, Inc.). We micropatterned a 1.8-μm-thick insulative photoepoxy layer (SU-8; Microchem Corp.) over the lower ITO-coated slide by spin-coating and photolithographic UV exposure through transparency masks printed at 8,000 d.p.i. (CAD/Art Services).

We cured all electrode arrays (**Supplementary Fig. 1**) at 185 °C for 1 h to complete cross-linking and immersed them in distilled water overnight to ensure SU-8 film biocompatibility. Treatment of internal chamber surfaces with tridecafluoro-1,1,2,2-tetrahydrooctyl)-1-trichlorosilane (United Chemical Technologies) prevented adhesion of crosslinked hydrogels, whereas treatment with 3-(trimethoxysilyl) propyl methacrylate (Sigma-Aldrich) promoted hydrogel attachment by providing free surface-bound groups that crosslink with the polymer. We sterilized the assembled chambers with 70% ethanol and flushed them with 1% (wt/vol) Pluronic F108 (BASF) to resist protein adsorption and decrease cell adhesion. Next we introduced the prepolymer cell suspension through fluidic ports (NanoPort; Upchurch). A function generator (Agilent 33120A) established the oscillating chamber bias. We monitored the applied a.c. voltage via an oscilloscope (TDS2014; Tektronix) connected in parallel. A broadband UVA lamp (365 nm; Glo-Mark Systems) illuminated the chamber from above to crosslink the hydrogel. The closed chamber prevented oxygen quenching of the polymerization reaction.

Hydrogel materials. We dissolved lyophilized poly(ethylene glycol) diacrylate (PEG-DA, 3.4 kDa; Nektar Therapeutics) in a custom electropatterning buffer (10 mM HEPES, 0.1 mM $CaCl_2$, 59 mM D-glucose and 236 mM sucrose; pH 7.35) with low ionic strength (conductivity: 21.4 mS/m) to promote rapid dielectrophoretic cell patterning[10,17]. The prepolymer solution contained final concentrations of 15% (wt/vol) PEG-DA, 0.03% (wt/vol) 1-[4-(2-hydroxyethoxy)-phenyl]-2-hydroxy-2-methyl-1-propane-1-one (Irgacure 2959 photoinitiator; Ciba), and 1% (wt/vol) bovine serum albumin to block nonspecific cell adhesion. We added cells (typically 10 million/ml) to the prepolymer immediately prior to patterning. Preparation of DCP hydrogels in thermogelling agarose is described in **Supplementary Methods**.

Hydrogel and cell characterization. We imaged cross-linked DCP hydrogels by epifluorescence, Hoffman modulation contrast and confocal microscopy. For fluorescent identification (**Fig. 1e**,**g**), we labeled cells with CellTracker dyes (Molecular Probes) before patterning. We quantified the numbers of cells per cluster and per hydrogel area (**Figs. 3** and **4**) with a semi-automated cell-counting program that used an intensity-based algorithm (MetaMorph Image Analysis), and verified the data from several microscope fields per experiment with manual counts. We assessed cell viability using the calcein AM and ethidium homodimer Live/Dead fluorescent stains (Molecular Probes), and cell counting (MetaMorph). All images are unprocessed or uniformly adjusted for brightness and contrast, except for one pseudocolored cluster of **Figure 1d**.

Chondrocyte DCP hydrogels. A description of the isolation of primary articular chondrocytes from bovine calf condyles is available in **Supplementary Methods**. The culture medium for chondrocyte DCP hydrogels contained Dulbecco's modified Eagle medium with 10% fetal bovine serum and additives (100 U/ml penicillin, 100 μg/ml streptomycin, 0.25 μg/ml Fungizone, 0.1 mM MEM nonessential amino acids, 0.4 mM L-proline, 2 mM L-glutamine), further supplemented with ascorbate (to promote chondrocyte matrix biosynthesis) at 100 μg/ml for 1 d and then reduced to 50 μg/ml. We maintained the hydrogels for 14 d in 0.6 ml medium per gel, changed every 2 d, in a humidified 5% CO_2 incubator at 37 °C. We measured the deposition of sGAG with the Alcian Blue dye binding assay, described in detail in **Supplementary Methods**. Briefly, we fixed DCP hydrogels and selectively stained them for sGAG as in **Figure 5b**. Next we divided the hydrogels into small fragments, each containing a distinct cell organization. We analyzed dye extracts from each fragment for absorbance (605 nm) and normalized to standard curves, fragment volume and cell density. Effects of cluster size among "sham" and patterned hydrogels were compared by ANOVA and Bonferroni's multiple comparison test. All data are mean ± s.d. unless noted.

Additional methods. Detailed methods regarding chondrocyte isolation and culture, the chondrocyte matrix biosynthesis assay and the patterning of cells within thermogelling hydrogels are available in **Supplementary Methods**.

Note: Supplementary information is available on the Nature Methods website.

ACKNOWLEDGMENTS

We acknowledge B. Schumacher for help adapting biochemical assays, S. Khetani, T. Klein, M. Blewis, and M. Voegtline for helpful discussion and for providing materials, K. Jadin for providing imaging code, and J. Elisseeff and K. Anseth for hydrogel assistance. We thank K. Hudson and M. Akiyama for providing hepatocytes, M. Weiss and H. Strick-Marchand for providing BMEL cells, and S. Mittal for fabricating the branching array. Funding was provided by The Whitaker Foundation (D.R.A. fellowship), the US National Science Foundation, the National Institutes of Health, the David and Lucille Packard Foundation and the National Aeronautics and Space Administration.

COMPETING INTERESTS STATEMENT

The authors declare that they have no competing financial interests.

Published online at http://www.nature.com/naturemethods/
Reprints and permissions information is available online at http://npg.nature.com/reprintsandpermissions/

1. Mueller-Klieser, W. Three-dimensional cell cultures: from molecular mechanisms to clinical applications. *Am. J. Physiol.* **273**, C1109–C1123 (1997).
2. Weaver, V.M. *et al.* β4 integrin–dependent formation of polarized three-dimensional architecture confers resistance to apoptosis in normal and malignant mammary epithelium. *Cancer Cell* **2**, 205–216 (2002).
3. Tanaka, H. *et al.* Chondrogenic differentiation of murine embryonic stem cells: effects of culture conditions and dexamethasone. *J. Cell. Biochem.* **93**, 454–462 (2004).
4. Benya, P.D. & Shaffer, J.D. Dedifferentiated chondrocytes reexpress the differentiated collagen phenotype when cultured in agarose gels. *Cell* **30**, 215–224 (1982).
5. Bhatia, S.N., Balis, U.J., Yarmush, M.L. & Toner, M. Effect of cell-cell interactions in preservation of cellular phenotype: cocultivation of hepatocytes and nonparenchymal cells. *FASEB J.* **13**, 1883–1900 (1999).
6. Khademhosseini, A., Langer, R., Borenstein, J. & Vacanti, J.P. Microscale technologies for tissue engineering and biology. *Proc. Natl. Acad. Sci. USA* **103**, 2480–2487 (2006).
7. Elisseeff, J. *et al.* Photoencapsulation of chondrocytes in poly(ethylene oxide)-based semi-interpenetrating networks. *J. Biomed. Mater. Res.* **51**, 164–171 (2000).
8. Bryant, S.J. & Anseth, K.S. Hydrogel properties influence ECM production by chondrocytes photoencapsulated in poly(ethylene glycol) hydrogels. *J. Biomed. Mater. Res.* **59**, 63–72 (2002).
9. Kelm, J.M., Timmins, N.E., Brown, C.J., Fussenegger, M. & Nielsen, L.K. Method for generation of homogeneous multicellular tumor spheroids applicable to a wide variety of cell types. *Biotechnol. Bioeng.* **83**, 173–180 (2003).
10. Jones, T.B. *Electromechanics of particles* (Cambridge University Press, Cambridge, New York, 1995).
11. Gascoyne, P.R. & Vykoukal, J. Particle separation by dielectrophoresis. *Electrophoresis* **23**, 1973–1983 (2002).
12. Voldman, J., Gray, M.L., Toner, M. & Schmidt, M.A. A microfabrication-based dynamic array cytometer. *Anal. Chem.* **74**, 3984–3990 (2002).
13. Gray, D.S., Tan, J.L., Voldman, J. & Chen, C.S. Dielectrophoretic registration of living cells to a microelectrode array. *Biosens. Bioelectron.* **19**, 1765–1774 (2004).

14. Lutolf, M.P. & Hubbell, J.A. Synthetic biomaterials as instructive extracellular microenvironments for morphogenesis in tissue engineering. *Nat. Biotechnol.* **23**, 47–55 (2005).
15. Nguyen, K.T. & West, J.L. Photopolymerizable hydrogels for tissue engineering applications. *Biomaterials* **23**, 4307–4314 (2002).
16. Liu, V.A. & Bhatia, S.N. Three-dimensional photopatterning of hydrogels containing living cells. *Biomedical Microdevices* **4**, 257–266 (2002).
17. Albrecht, D.R., Sah, R.L. & Bhatia, S.N. Geometric and material determinants of patterning efficiency by dielectrophoresis. *Biophys. J.* **87**, 2131–2147 (2004).
18. Williams, C.G., Malik, A.N., Kim, T.K., Manson, P.N. & Elisseeff, J.H. Variable cytocompatibility of six cell lines with photoinitiators used for polymerizing hydrogels and cell encapsulation. *Biomaterials* **26**, 1211–1218 (2005).
19. Jadin, K.D. *et al.* Depth-varying density and organization of chondrocytes in immature and mature bovine articular cartilage assessed by 3D imaging and analysis. *J. Histochem. Cytochem.* **53**, 1109–1119 (2005).
20. Mankin, H.J., Dorfman, H., Lippiello, L. & Zarins, A. Biochemical and metabolic abnormalities in articular cartilage from osteo-arthritic human hips. II. Correlation of morphology with biochemical and metabolic data. *J. Bone Joint Surg. Am.* **53**, 523–537 (1971).
21. Wilkins, R.J., Browning, J.A. & Urban, J.P. Chondrocyte regulation by mechanical load. *Biorheology* **37**, 67–74 (2000).
22. van der Kraan, P.M., Buma, P., van Kuppevelt, T. & van den Berg, W.B. Interaction of chondrocytes, extracellular matrix and growth factors: relevance for articular cartilage tissue engineering. *Osteoarthritis Cartilage* **10**, 631–637 (2002).
23. Archer, S., Li, T.T., Evans, A.T., Britland, S.T. & Morgan, H. Cell reactions to dielectrophoretic manipulation. *Biochem. Biophys. Res. Commun.* **257**, 687–698 (1999).
24. Docoslis, A., Kalogerakis, N. & Behie, L.A. Dielectrophoretic forces can be safely used to retain viable cells in perfusion cultures of animal cells. *Cytotechnology* **30**, 133–142 (1999).
25. Graff, R.D., Kelley, S.S. & Lee, G.M. Role of pericellular matrix in development of a mechanically functional neocartilage. *Biotechnol. Bioeng.* **82**, 457–464 (2003).
26. Gagne, T.A. *et al.* Enhanced proliferation and differentiation of human articular chondrocytes when seeded at low cell densities in alginate in vitro. *J. Orthop. Res.* **18**, 882–890 (2000).
27. Iwasa, J. *et al.* Effects of cell density on proliferation and matrix synthesis of chondrocytes embedded in atelocollagen gel. *Artif. Organs* **27**, 249–255 (2003).
28. Quintavalla, J., Kumar, C., Daouti, S., Slosberg, E. & Uziel-Fusi, S. Chondrocyte cluster formation in agarose cultures as a functional assay to identify genes expressed in osteoarthritis. *J. Cell. Physiol.* **204**, 560–566 (2005).
29. Handley, C.J. & Lowther, D.A. Extracellular matrix metabolism by chondrocytes. III. Modulation of proteoglycan synthesis by extracellular levels of proteoglycan in cartilage cells in culture. *Biochim. Biophys. Acta* **500**, 132–139 (1977).
30. Strick-Marchand, H. & Weiss, M.C. Inducible differentiation and morphogenesis of bipotential liver cell lines from wild-type mouse embryos. *Hepatology* **36**, 794–804 (2002).

Supplementary Figure 1.

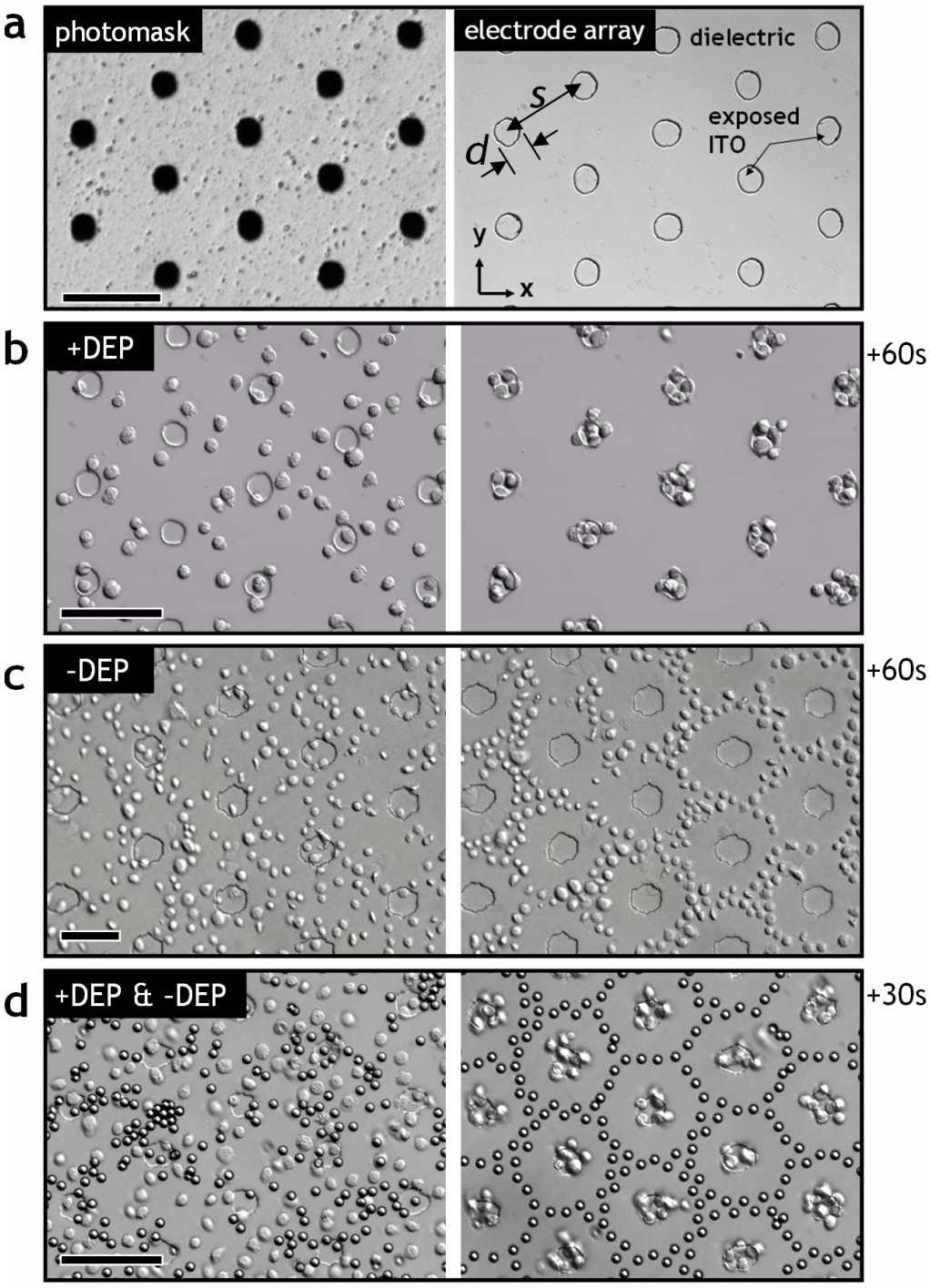

Supplementary Figure 1. DEP micropatterning of cells and microspheres. (**a**) The hexagonal photomask pattern is accurately reproduced in the microfabricated electrode array with electrode spacing, *s*, and diameter, *d*. (**b**) During positive DEP patterning, Swiss 3T3 fibroblasts move toward high electric field strength at the electrodes, *s* = 100 μm apart, within a 15% (wt/vol) PEG-DA prepolymer (viscosity: 3.3 cP) after 60 s exposure to 3.0 V_{rms} at 3.0 MHz (also depicted in **Supplementary Video 1**). (**c**) During negative DEP patterning at low bias frequency (10 kHz, see **Supplementary Fig. 3**), identical cells move away from the electrodes (*s* = 150 μm) into a honeycomb pattern, after 60 s exposure at 3.0 V_{rms}. (**d**) A heterogeneous mixture of NIH 3T3 fibroblasts and polystyrene microspheres in polymer-free buffer simultaneously separate and electropattern after 30 s exposure to 5.3 V_{rms} at 3.0 MHz. See **Supplementary Video 2**. Patterning is faster in (**d**) compared with (**b**) because DEP force increases with the square of the applied potential, and patterning speed is inversely proportional to suspending fluid viscosity[1]. Scale bars, 100 μm.

1. Albrecht, D. R., Sah, R. L. & Bhatia, S. N. Geometric and material determinants of patterning efficiency by dielectrophoresis. *Biophys J* **87**, 2131–47 (2004).

Supplementary Figure 2.

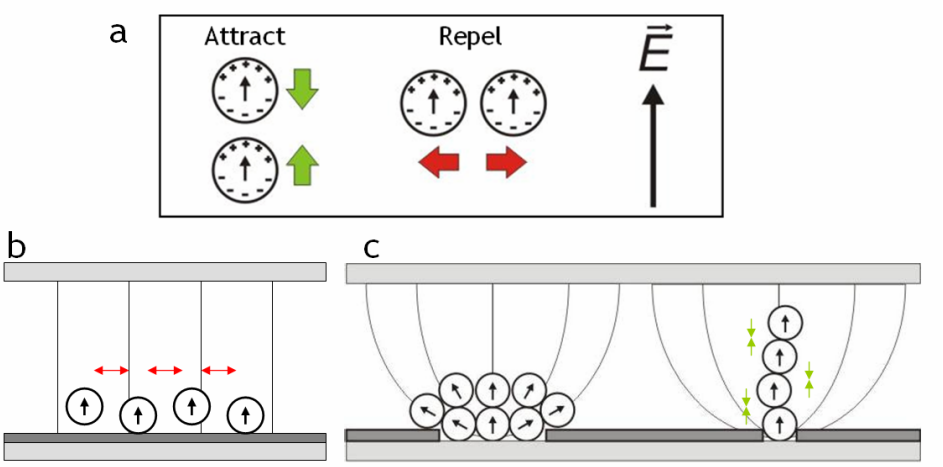

Supplementary Figure 2. Cell-cell forces in electric fields. (**a**) Cells aligned with the electric field attract while those aligned perpendicular to the electric field repel, due to interactions between induced dipoles. (**b**) In unclustered regions without gaps in the dielectric layer (e.g. **Fig. 4a**, U), a weak uniform electric field perpendicular to the electrode array weakly repels cells (red arrows) and promotes single cell organization. (**c**) In patterned regions, 3-D cell cluster shape may vary from flattened spheroids (*left*) to linear columns (*right*), as in **Fig. 1e** and **Fig. 1f**, respectively. Linear cell columns form due to the dominance of cell-cell attractive forces (green arrows) over DEP patterning force. Prior to hydrogel crosslinking, these linear structures are less stable and may collapse in the presence of convective flow.

Supplementary Figure 3.

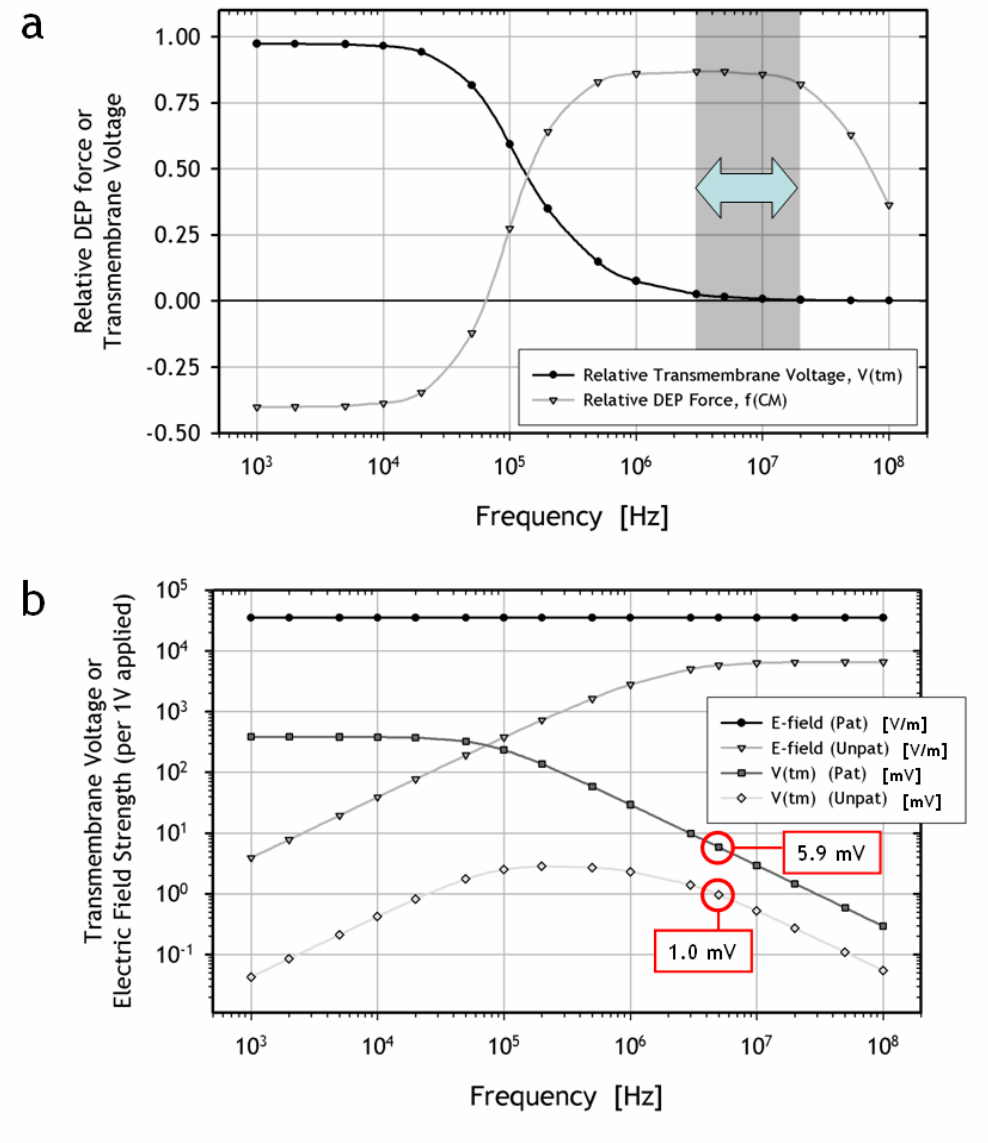

Supplementary Figure 3. Frequency dependence of relative DEP force and induced transmembrane voltage during DEP electropatterning. (**a**) Maximum relative DEP force in electropatterning buffer and minimal induced transmembrane potential is achieved in the frequency range of ~3–20 MHz (shaded). Data are plotted from equations (1) and (2) below. (**b**) Estimated maximum electric field strength and transmembrane potential for the chamber geometry used in these studies. At 5.0 MHz used in the chondrocyte studies (**Fig. 5**), we estimate that field-induced transmembrane potentials did not exceed 2.2 mV_{rms} (Unpatterned, 'U') or 13.3 mV_{rms} (Patterned clusters, 'II') during the 2.25 ± 0.13 V_{rms} chamber bias. Data are plotted from equations (3) and (4) below.

Supplementary Figure 3 Notes. Relative DEP force is given by the real portion of the Clausius-Mossotti factor, a complex scaling term that represents the relative permittivity between the particle (p) and the suspending fluid (fl). For a cell, approximated as a single shell sphere, relative DEP force is[1]:

$$\tilde{f}_{CM}(\omega)=\frac{\tilde{\varepsilon}_p-\tilde{\varepsilon}_{fl}}{\tilde{\varepsilon}_p+2\tilde{\varepsilon}_{fl}};\quad \tilde{\varepsilon}_p=\tilde{\varepsilon}_i\frac{R^3(\tilde{\varepsilon}_i+2\tilde{\varepsilon}_m)+2(R-d_m)^3(\tilde{\varepsilon}_i-\tilde{\varepsilon}_m)}{R^3(\tilde{\varepsilon}_i+2\tilde{\varepsilon}_m)-(R-d_m)^3(\tilde{\varepsilon}_i-\tilde{\varepsilon}_m)}, \tag{1}$$

where $\tilde{\varepsilon}=\varepsilon+\sigma/j\omega$ is the complex permittivity, $j=(-1)^{1/2}$, and values typical of mammalian cells[2] are listed in **Table 1** below. The maximal induced transmembrane potential is[3]:

$$V_{tm}(\omega)=1.5\left|\boldsymbol{E}_{fl}\right|R\left[1+\frac{G_s}{\sigma_{fl}R}+\frac{R}{d_m}(\sigma_m+j\omega\varepsilon_m)\left(\rho_i+\frac{1}{2\sigma_{fl}}+\frac{G_s}{\sigma_{fl}\sigma_i R}\right)\right]^{-1}, \tag{2}$$

where the bracketed term represents relative transmembrane potential plotted in **Supplementary Fig. 3a**.

Table 1. Cell parameters for calculating Calusius-Mossotti factor

		Unit	Internal (i)	Membrane (m)	Fluid (fl)
Conductivity	σ	(S m^{-1})	0.5	3 x 10^{-6}	0.0214
Permittivity	ε	ε_0	50	8	80
Surface conductance	G_s	(S m^{-2})		10^{-9}	
Cell Radius	R	[m]		7.5 x 10^{-6}	
Membrane thickness	d_m	[m]		8 x 10^{-9}	

The maximum electric field magnitude, $\left|\boldsymbol{E}_{fl}\right|$, was determined by finite element modeling for patterned regions (CFD-ACE+, CFDRC, Huntsville, AL) and assumed to be invariant with frequency. However, in unpatterned regions where the dielectric layer is intact, the bias applied across the chamber is attenuated in a frequency-dependent manner. Neglecting the impedance of electrical connections, the bias across the fluid, V_{fl}, relates to the applied voltage, V_{app}, by:

$$\frac{V_{fl}}{V_{app}} = \frac{\left|Z_{fl}\right|}{\left|Z_{fl}\right| + \left|Z_{di}\right|}. \tag{3}$$

We consider each volume, fluid (fl) and dielectric (di), to be a thin, homogeneous rectangular slab of thickness h, area A, resistivity ρ, permittivity ε, and impedance magnitude:

$$\left|Z_x\right| = \frac{h_x}{A}\frac{\rho_x}{\omega\varepsilon_x}\left(\rho_x^2 + \frac{1}{\omega^2\varepsilon_x^2}\right)^{-1/2}. \tag{4}$$

Electric field strength was calculated as $\left|E_{fl}\right| = \left|V_{fl}\right| / h_{fl}$ for unpatterned regions. The following properties were used to calculate the results in **Supplementary Fig. 3**.

Table 2. Parameters for calculating impedance of dielectric layer

		Unit	Fluid layer	Dielectric layer
Thickness	h	(μm)	100	2.0
Resistivity	ρ	(Ω m)	46.7	10^9
Permittivity	ε	ε_0	80	3

REFERENCES

1. Jones, T. B. *Electromechanics of particles* (Cambridge University Press, Cambridge; New York, 1995).

2. Fuhr, G., Glasser, H., Muller, T. & Schnelle, T. Cell manipulation and cultivation under a.c. electric field influence in highly conductive culture media. *Biochim Biophys Acta* **1201**, 353–60 (1994).

3. Grosse, C. & Schwan, H. P. Cellular membrane-potentials induced by alternating-fields. *Biophysical Journal* **63**, 1632–1642 (1992).

Supplementary Figure 4.

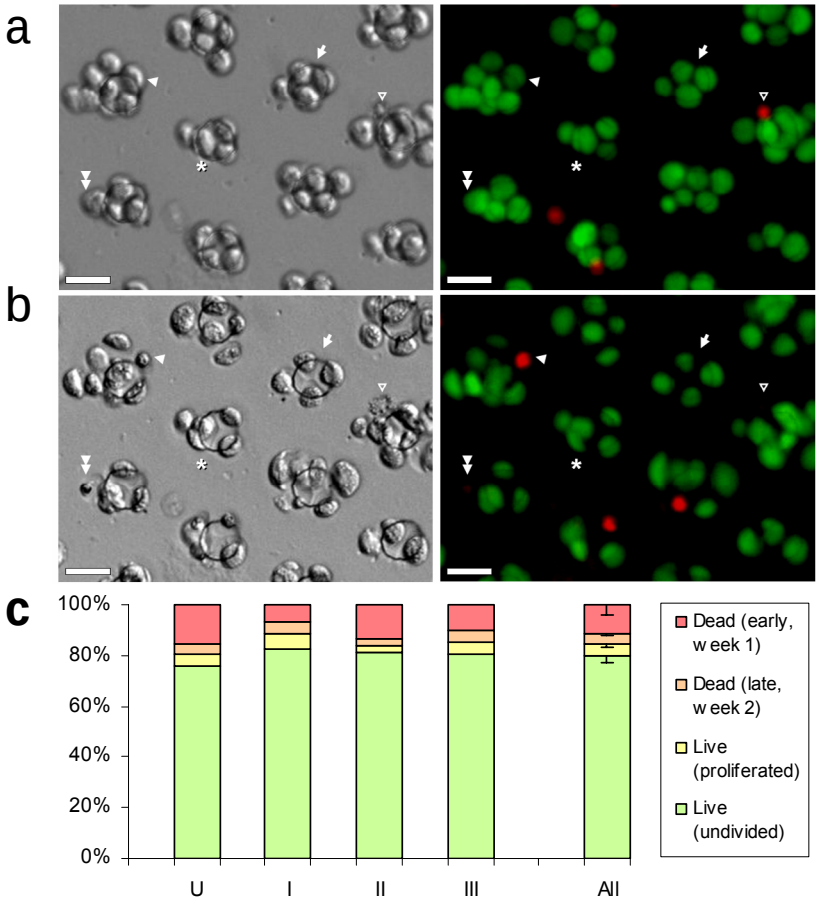

	Cell Fate	U	I	II	III	All
➔	Live (undivided)	76%	82%	81%	80%	80 ± 3%
*	Live (proliferated)	5%	6%	2%	5%	5 ± 1%
►	Dead (late, week 2)	4%	5%	3%	4%	4 ± 1%
▶▶	Dead (early, week 1)	16%	6%	13%	10%	11 ± 4%
	cells tracked	141	154	166	137	598

Supplementary Figure 4. Fate of hydrogel-embedded chondrocytes over 14 days. Identical regions of a DCP hydrogel stained for viability at day 1 (**a**) and again at day 14 (**b**) are shown in Hoffman contrast (left) and epifluorescence (right). Initially viable cells (green) were tracked to determine changes in morphology, viability, and proliferation (**c**). Organizations U (unclustered) and I-III (clusters) are as in **Fig. 5**; "All" represents mean ± s.d. for all organizations. Most cells viable at 14 days did not proliferate (95 ± 2% s.d.), due to the nondegradable PEG hydrogel, and no cell migration was observed. No differences in cell fate were observed among cell organizations. Cells that became nonviable over time in culture were classified as early- or late-death, depending on the absence or presence of nuclear staining material (red) at day 14, respectively (DNA of dead cells degraded over ~1 week). Scale bars, 25 μm.

Supplementary Figure 5.

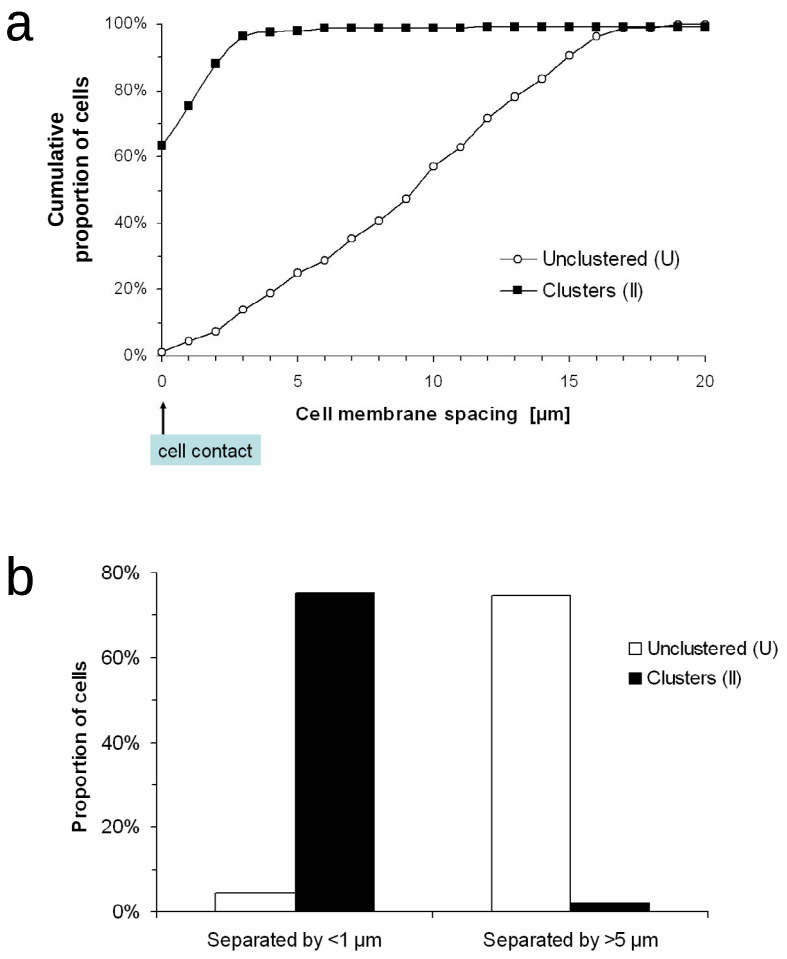

Supplementary Figure 5. Minimum separation distance between adjacent cells in patterned hydrogels. DCP hydrogels containing fluorescently-stained chondrocytes were analyzed by automated image segmentation to determine the spacing between each cell and its nearest neighbor. Data were obtained from unclustered (U) and clustered (II) fields shown in **Fig. 4a**. (**a**) Cumulative proportion of cells within a specifed cell spacing. (**b**) Whereas 75% of clustered cells were in contact or separated by less than 1 µm, an equal proportion of unclustered cells were separated by greater than 5 µm (average 9 ± 5 µm s.d.).

SUPPLEMENTARY METHODS

Chondrocyte isolation and culture. Primary bovine calf condylar chondrocytes were isolated as previously described[1]. Briefly, full-thickness articular cartilage slices were harvested from the femoral condyles of 6 bovine calves, 1–3 weeks old, and chondrocytes were isolated by sequential digestion for 1 hr with 0.2% (wt/vol) pronase (Sigma) and 16 hr with 0.016% (wt/vol) collagenase P (Roche Diagnostics). Chondrocytes were maintained in 3D alginate culture until use to stabilize cell phenotype[2]. Chondrocytes were resuspended in 1.2% (wt/vol) alginate (Keltone LV, Kelco) in 150 mM NaCl at 4 million cells mL^{-1}, and then expressed from a 22-gage needle into 102 mM $CaCl_2$ to polymerize small alginate beads containing encapsulated chondrocytes. The beads were cultured in DMEM/F12 with 10% fetal bovine serum (FBS) and additives (100 U mL^{-1} penicillin, 100 µg mL^{-1} streptomycin, 0.25 µg mL^{-1} Fungizone, 0.1 mM MEM non-essential amino acids, 0.4 mM L-proline, 2 mM L-glutamine) for 2–3 weeks with medium changes every 2–3 days (1 mL per million cells per day). Chondrocytes released from alginate using 55 mM sodium citrate in 150 mM NaCl retain a cell-associated matrix (CM) rich in collagen and proteoglycans[3]. For most experiments, the CM was stripped immediately prior to use to allow direct cell-cell interaction, by incubation with 2 mg mL^{-1} collagenase B (Roche) in DMEM with 10% FBS and additives for 4 hr at 37 ºC under constant gentle stirring[4]. In one study (Discussion), cells with or without the CM were compared in patterned DCP hydrogels.

Matrix biosynthesis assay. The deposition of sulfated glycosaminoglycans (sGAG) by chondrocytes embedded within DCP hydrogels was characterized spatially and quantitatively via selective binding of Alcian Blue, a cationic dye. Hydrogels were washed twice with saline, fixed in 10% neutral-buffered formalin for 10 minutes, and incubated with a solution of 0.5% (wt/vol) Alcian Blue (8GX, Sigma) in 0.1N HCl in

water, pH 1.0, for 3.5–4 hr on a shaker. Hydrogels were then rinsed at least 5 times in water to remove unbound dye and imaged by brightfield microscopy or stored at 4 ºC in saline. To quantify bulk sGAG deposition, stained hydrogels were trimmed to separate quadrants of distinct cell organization, and further into approximately 10–20 mm^2 sections. Section area was quantified via microscopy to normalize sGAG data to hydrogel volume and to cell number via measured volumetric seeding density. The Alcian Blue dye was disassociated from each hydrogel section in 100 µl Extraction Buffer (4 M guanidinium chloride, 50 mM Trizma-HCl, 0.1% (wt/vol) CHAPS (Sigma), pH 7.4) for 12–16 hr at room temperature on a shaker, transferred to a 96-well plate, and analyzed spectrophotometrically at 605 nm. Standard curves were formed using control hydrogel disks containing known concentrations of sGAG extracted from bovine calf articular cartilage using the procedure of Roughley et al.[5] and quantified as previously described[6]. Absorbance values correlated linearly with proteoglycan concentration from 0–4.0 mg mL^{-1} (R^2 = 0.998), a range that spanned all DCP hydrogel sections.

DCP within thermogelling hydrogels. To demonstrate method compatibility with alternative hydrogels, cells were patterned within agarose hydrogels (**Fig. 2h,i**). Agarose (Type IX-A: Ultra-low Gelling Temperature, Sigma) was dissolved in the electropatterning buffer by boiling and allowed to cool before mixing with an equal volume of the cell suspension. The prepolymer cell suspension, containing 1% (wt/vol) agarose, was introduced into the patterning chamber following sterilization and flushing with buffer and cell-free agarose. The chamber was maintained at 25–37 ºC during cell patterning, and then immediately cooled in ice water for 5 minutes to initiate agarose gelation. The cell-patterned agarose hydrogels were removed from the chamber and remained gelled in 37 ºC culture.

REFERENCES

1. Mok, S. S., Masuda, K., Hauselmann, H. J., Aydelotte, M. B. & Thonar, E. J. Aggrecan synthesized by mature bovine chondrocytes suspended in alginate. Identification of two distinct metabolic matrix pools. *J Biol Chem* **269**, 33021–7 (1994).

2. Hauselmann, H. J. et al. Synthesis and turnover of proteoglycans by human and bovine adult articular chondrocytes cultured in alginate beads. *Matrix* **12**, 116–29 (1992).

3. Masuda, K., Sah, R. L., Hejna, M. J. & Thonar, E. J. A novel two-step method for the formation of tissue-engineered cartilage by mature bovine chondrocytes: the alginate-recovered-chondrocyte (ARC) method. *J Orthop Res* **21**, 139–48 (2003).

4. van Osch, G. J., van der Veen, S. W., Buma, P. & Verwoerd-Verhoef, H. L. Effect of transforming growth factor-beta on proteoglycan synthesis by chondrocytes in relation to differentiation stage and the presence of pericellular matrix. *Matrix Biol* **17**, 413–24 (1998).

5. Roughley, P. J. & White, R. J. Age-related changes in the structure of the proteoglycan subunits from human articular cartilage. *J Biol Chem* **255**, 217–24 (1980).

6. Farndale, R. W., Sayers, C. A. & Barrett, A. J. A direct spectrophotometric microassay for sulfated glycosaminoglycans in cartilage cultures. *Connect Tissue Res* **9**, 247–8 (1982).